A priori analysis of sub-grid variance of a reactive scalar using DNS data of high Ka flames

Thommie Nilsson, Ivan Langella, Nguyen Anh Khoa Doan, Nedunchezhian Swaminathan, Rixin Yu & Xue-Song Bai

Published online: 04 Apr 2019.

Submit your article to this journal ⧉

View Crossmark data ⧉

Taylor & Francis
Taylor & Francis Group

Check for updates

A priori analysis of sub-grid variance of a reactive scalar using DNS data of high Ka flames

Thommie Nilsson [a]*, Ivan Langella[b,c], Nguyen Anh Khoa Doan [b],
Nedunchezhian Swaminathan[b], Rixin Yu[a] and Xue-Song Bai[a]

[a]Department of Energy Sciences, Lund University, Lund, Sweden; [b]Department of Engineering, University of Cambridge, Cambridge, UK; [c]Department of Aeronautical and Automotive Engineering, Loughborough University, Loughborough, UK

Direct numerical simulations (DNS) of low and high Karlovitz number (Ka) flames are analysed to investigate the behaviour of the reactive scalar sub-grid scale (SGS) variance in premixed combustion under a wide range of combustion conditions (regimes). An order of magnitude analysis is performed to assess the importance of various terms in the variance evolution equation and the analysis is validated using the DNS results. This analysis sheds light on the relative behaviour among turbulent transport and production, scalar dissipation and chemical processes involved in the evolution of the SGS variance at different Ka. The common expectation is that the variance equation shifts from a reaction-dissipation balance at low Ka to a production–dissipation balance at high Ka with diminishing reaction contribution. However, in large eddy simulation (LES), a high Ka alone does not make the reaction term negligible, as the relative importance of the reaction term has a concurrent increase with filter size. The filter size can be relatively large compared with the Kolmogorov length scale in practical LES of high Ka flames, and as a consequence a reaction–production–dissipation balance may prevail in the variance equation even in a high Ka configuration, and this possibility is quantified using the DNS analysis in this work. This has implications from modelling perspectives, and therefore two commonly used closures in LES for the SGS scalar dissipation rate are investigated *a priori* to estimate the importance of the above balance in LES modelling. The results are explained to highlight the interplay among turbulence, chemistry and dissipation processes as a function of Ka.

Keywords: scalar variance; scalar dissipation rate; turbulent premixed flame; direct numerical simulation; high Karlovitz number

1.   Introduction

Fuel-lean premixed combustion has the potential to improve thermal efficiency and reduce NO_x emissions [1,2] but it is highly susceptible to combustion instability, blowout and flashback [3]. To enable its use, a better understanding of its physics is required. The presence of intense turbulence with lean flames in practical applications such as gas turbines typically yields high Karlovitz numbers, Ka, which is defined as the ratio between the chemical time scale and the smallest turbulence time scale. This situation of strong

turbulence and lower reactivity yields complex physics with reaction zones broadening [4,5] and local extinction [5,6]. Thus, it is imperative to gain better understanding of high Ka flames and their modelling for the design of future lean-burn combustors.

Given the difficulty of performing measurements under high Ka conditions, direct numerical simulation (DNS) provides the necessary physical insights and an opportunity for a priori analysis of sub-grid scale (SGS) models for large eddy simulation (LES). Several recent DNS studies of high Ka flames have highlighted how the structure of the flame is broadened and disturbed [7–10], but it has also been shown that, probably due to thermal expansion effects [11], the transition to the broken reaction zone regime happens at a much higher Karlovitz number than the traditionally predicted value of 100 [12–17]. There have also been published studies that have investigated the effect of flame stretch and mean shear [18,19], differential diffusion and non-unity Lewis number [7,16,20] and Soret and Dufour effects [20] on the flame. It is known that small-scale turbulence can enter and disturb the reaction zone if the Ka is large enough, and that differential diffusion can affect the flame structure at high Ka.

In LES, large-scale turbulent eddies are resolved down to a cut-off scale while the effect of sub-grid scales requires modelling. For turbulent premixed combustion, this modelling becomes more important as most of the chemical reactions occur at the sub-grid scale. LES models that are based on a reaction progress variable, c, [21–25] and are of interest in our a priori analysis, describe the flame using a resolved reaction progress variable, $\tilde{c}$, and its SGS variance, $\sigma_c^2 = \widetilde{c^2} - \widetilde{c}^2$. For example, Lapointe et al. [26] showed in an a priori analysis that tabulated chemistry with presumed probability density function (PDF) parameterized by $\tilde{c}$ and σ_c^2 was able to provide a reasonable prediction of the reaction rate for high Ka flames. That study included flames up to Ka = 740.

Indeed, the sub-grid variance of the reaction progress variable has been shown to be strongly influenced by reaction, diffusion, dissipation, convection and their interactions at the SGS level [2] and the intense turbulence/flame interaction could greatly affect the evolution of σ_c^2 in high Ka flames. It is not fully understood how the relative importance of the various terms appearing in the transport of SGS variance changes in different regimes, an important question for the $\tilde{c}$-based models. Thus, the objective of this work is to investigate the behaviour of the SGS variance equation and its modelling in high Karlovitz number flames. For this purpose, DNS data of lean premixed methane-air flames with complex chemistry having Ka ranging from 4 up to 4100 is analysed. First, the importance of the various terms in the SGS variance equation is assessed and their behaviours with Ka are studied. Second, the existing models for the closure of the reaction, production and dissipation terms in the SGS variance equation are analysed and compared.

In Section 2, the DNS data and numerical procedures are presented. In Section 3, the transport equation of SGS variance of the reaction progress variable and related models are introduced, and the behaviour of various terms involved in the equation at different Ka are assessed using an order-of-magnitude analysis. Section 4.1 presents DNS analysis of the terms in the SGS variance equation, and Section 4.2 presents a priori evaluation of the related models.

2. Numerical simulations and data processing

Four DNS cases of statistically planar premixed flames of methane-air mixture at fuel-lean ($\phi = 0.6$), atmospheric pressure, and different turbulence intensity (Karlovitz numbers) are studied. Three out of the four cases (K100, K800 and K4100) are the same as those
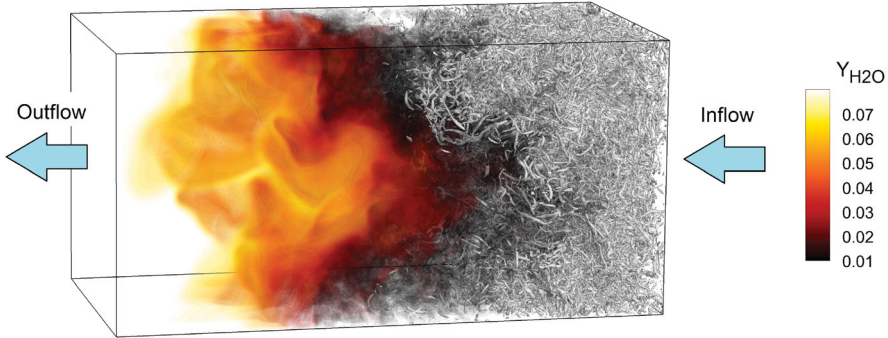
Figure 1. Illustration of case K4100. Translucent iso-surfaces of H$_2$O shows the flame brush and the iso-surface of $\lambda_2 = -4 \times 10^{11}$ s^{-1} shows vortical structures.

presented in [27], but with an increased simulation time. Thus, the quantitative results presented in [27] are relevant also for the current data set. The fourth case, K4, is new but uses the exact same configuration as the other cases except for the smaller turbulence intensity.

The simulation configuration involves an initially flat flame propagating in a rectangular channel of dimensions $10 \times 5 \times 5$ mm. Figure 1 illustrates the set-up for the highest Ka number case: the flame region is highlighted by an ensemble of translucent iso-surfaces of H$_2$O mass fraction and vortical structures are identified by an iso-surface of λ_2 which is the intermediate eigenvalue of the strain rate tensor, S_{ij} [28].

Periodic boundary conditions are imposed in the cross-stream directions and a zero-gradient boundary condition is imposed on the outlet boundary. For the inlet boundary, constant values of temperature ($T = 298$ K) and species are imposed while a turbulence boundary condition is used for the velocity components as described below.

To keep the flame near the centre of the domain, the mean velocity $u_{in}(t)$ perpendicular to the inlet is adjusted such that the domain average fuel mass fraction is 50% of the inlet value. On average this yields $u_{in} = X_L d(\langle Y_F \rangle / Y_{F,in})/dt$ where $\langle Y_F \rangle$ is the domain average fuel mass fraction, $Y_{F,in}$ is the fuel mass fraction at the inlet boundary and X_L is the domain length (distance from inlet to outlet). A lower limit of zero needs to be adopted for u_{in} to avoid numerical instabilities that can otherwise result from negative mean inlet velocity. The reason this is needed is that, in the early time of the simulation, the pre-heat zone is being broadened. This causes thermal expansion in the pre-heat zone which pushes the flame toward the outlet. The fluctuating velocity is given by extracting a section from a pre-generated turbulence field and the location where this section is extracted is moved through the pre-generated field at the speed u_{in} during the simulation. A homogeneous isotropic turbulence field for this purpose is generated as follows: A flow field with desired turbulence intensity and length scale is synthesised in a fully periodic cubic box by sampling sine waves of suitable wave numbers and amplitudes. The flow in this box is then simulated until a statistically stationary state is reached, quantified by convergence of the energy spectrum and the energy dissipation rate. During this simulation, the turbulence intensity and length scale are maintained by low-wavenumber forcing. The computed field is then stored and later used for the inlet boundary as well as the initial condition. The low-wavenumber forcing strategy used to pre-generate turbulence, which is also enabled during reactive simulations to maintain the turbulence intensity, works by

injecting energy to low-wavenumber modes through the addition of a source term in the momentum equation. Further details on this forcing method are provided in [29,30].

All reactive flow simulations were initiated by a flat flame profile centred in the domain. This profile was obtained from a one-dimensional laminar freely propagating flame computed using the same thermochemical parameters and the same numerical solver that were used for the turbulent flames. Initial condition for the velocity field is set to the pre-generated turbulence field.

The governing equations for conservation of mass, momentum, energy and chemical species at low Mach number are discretised on a uniform cartesian grid and solved using a DNS solver, see Yu et al. [31] for a detailed description of the implementation and validation. The use of a low Mach number formulation is acceptable since the velocities are small compared to the sound speed everywhere in the domain. A fifth-order weighted essentially non-oscillating (WENO) method is used for convective terms in the species and temperature equations while a 6th order central difference scheme is used for all other terms. The WENO method is used to improve the numerical stability in regions of strong gradients, such as across a flame. For time discretisation, a second order operator splitting scheme [32] is employed by performing integration of the chemical source terms between two half time-step integrations of the diffusion term. The integration of the diffusion term is further divided into smaller explicit steps to ensure stability and the overall time step is set to ensure a CFL number less than 0.1. Chemical source terms are integrated using the stiff DVODE solver [33]. The variable coefficient Poisson equation for pressure difference is solved using a multigrid method [34]. The skeletal chemical kinetic mechanism of Smooke and Giovangigli [35], which involves 16 species and 35 reactions, is used to model the combustion chemistry. Species diffusion coefficients, thermal conductivity and viscosity are mixture averaged based on the detailed properties for individual species obtained from the CHEMKIN thermodynamic database.

Important parameters for the different cases are summarised in Table 1. These include the turbulent intensity u'/S_L, Karlovitz number $\text{Ka} = (u'^3/S_L^3 \cdot \delta_{th}/\ell_0)^{1/2}$, Damköhler number $\text{Da} = \ell_0 S_L/(\delta_{th} u')$, the turbulence Reynolds number $\text{Re}_0 = u'\ell_0/v_u$ and the flame Reynolds number $\text{Re} = \text{Ka}^2 \text{Da}^2$. Here, u' is the root mean square velocity fluctuation, ℓ_0 is the integral length scale, $S_L = 0.121$ m/s is the laminar flame speed,

Table 1. Properties of the DNS data set: Integral length scale ℓ_0, Kolmogorov length scale η, velocity fluctuation u', turbulence intensity u'/S_L, Karlovitz number Ka, Damköhler number Da, Reynolds number Re_0, flame Reynolds number Re, ratio of flame thickness to Kolmogorov length scale, grid spacing h and number of grid cells N.

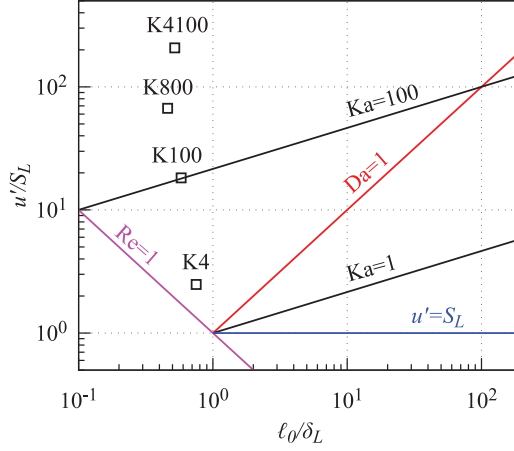| Case	K4	K100	K800	K4100
ℓ_0 (mm)	0.70	0.52	0.43	0.48
η (μm)	90	26	9.4	4.2
u' (m/s)	0.30	2.2	8.1	25
u'/S_L	2.5	18	67	210
Ka	4.5	100	800	4100
Da	0.30	0.032	0.0069	0.0025
Re_0	12	63	190	660
Re	1.9	11	31	110
δ_{th}/η	10	35	98	220
h (μm)	39.1	39.1	19.5	9.77
N	256×128^2	256×128^2	512×256^2	1024×512^2

Figure 2. Regime diagram for premixed flames showing the condition of the present DNS simulations.

$\delta_{th} = (T_b - T_u)/|\nabla T|_{\max} = 0.917$ mm is the laminar thermal flame thickness where b and u denote burned and unburned states, respectively, and $\eta = (\nu^3/\varepsilon)^{1/4}$ is the Kolmogorov length scale of the unburned mixture. The laminar flame properties were evaluated in the same one-dimensional steady flame that was used for the initial condition. The quantities shown in Table 1 are evaluated using time averaged turbulence properties from the pre-generated turbulence fields used for boundary and initial conditions. The number of mesh cells N used to discretise the domain is also reported in Table 1 for each of the cases; these were chosen such that $h \lesssim \delta_{th}/20$ and $h \lesssim 2.1\eta$ [36] to ensure that both the flame and the turbulence are adequately resolved. The regime diagram for premixed flames [37] is shown in Figure 2 illustrating that the cases span the regions traditionally considered to be the thin reaction zone and broken reaction zone regimes.

For the following analysis filtered quantities need to be computed from the DNS data. An LES filtered quantity, $\overline{\psi}$, is obtained by convolution with a Gaussian filter kernel as:

$$\overline{\psi}(\mathbf{x}, t) = \iiint_V \psi(\mathbf{r}, t) G_\Delta(\mathbf{x} - \mathbf{r}) \, d\mathbf{r} \qquad (1)$$

where ψ is the quantity to be filtered, V is the computational domain and $G_\Delta(\mathbf{r})$ is a Gaussian filter kernel with filter width Δ. Filter width is conventionally defined by $\Delta^2 = s^2/12$ where s^2 is the variance of the Gaussian function [36]. For computation reasons, and to minimise truncation errors, the convolution product is performed using a Fourier transform as $\widehat{\overline{\psi}}(\mathbf{k}) = \widehat{\psi}(\mathbf{k})\widehat{G}(\mathbf{k})$ where $\widehat{}$ denotes Fourier transform and $\mathbf{k}$ is the wave vector. To be able to use Fourier transform the domain first needs to be made fully periodic. This is accomplished by mirroring the domain in the non-periodic x-direction, which makes the data periodic. Density weighted (Favre) filtered quantities will also be needed and these are computed as $\widetilde{\psi} = \overline{\rho\psi}/\overline{\rho}$.

A reaction progress variable based on H_2O mass fraction, $c = Y_{H2O}/Y_{H2O,b}$, is used to describe the flame, where b denotes burned mixture. Instantaneous fields of c and its reaction rate $\dot{\omega}$ are shown for the four cases in Figure 3, taken near the end of each simulation. As Ka increases, the flame and in particular its pre-heat zone become more perturbed and broadened as observed in the figure. Consistent with previous studies [12–17] it takes a
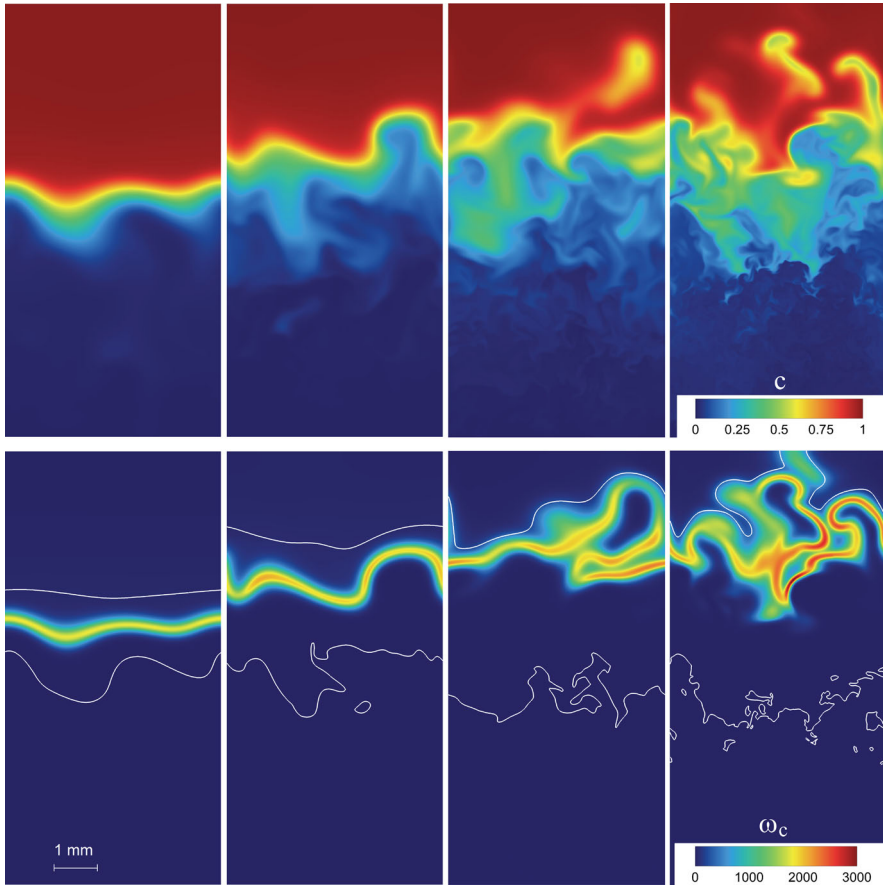
Figure 3. Progress variable c (top) and its reaction rate $\dot{\omega}_c$ [kg/m^3/s] (bottom). Cases from left to right: K4, K100, K800 and K4100. Lines show iso-contours corresponding to $c = 0.1$ and $c = 0.98$.

Karlovitz number much above 100, or a reaction layer Ka much above 1, before the reaction layer is disturbed by turbulence. At Ka = 800, the flame is folded at smaller scales, and curved regions with radius of curvature comparable to the flame thickness become common. At a Ka of 4100, the internal structure is seen to be perturbed and the geometry of the reaction layer is complex. Extensive flame folding can potentially lead to formation of islands, and small-scale mixing and straining create both broadened and thinned flame segments where reaction rates can locally be much higher than the peak value of its laminar counterpart. Large-scale flame folding can also happen at low Karovitz numbers but is restricted in these simulations due to domain size. All this complexity is a manifestation of the interaction between reaction, convection and diffusion as described by the transport equations, thus, a successful LES simulation depends on this balance being mimicked well.

The transport equation for SGS variance of c, which is needed in the reaction progress variable-based models of interest here, is also the result of interaction among reaction, convection and diffusion, and it is imperative to investigate this equation and its various terms in detail. This analysis is conducted in the next section.

3. Modelling of SGS variance

The transport equation for the SGS variance, $\sigma_c^2 = \widetilde{c^2} - \tilde{c}^2$, can be derived from the equation for c. This is done by first obtaining equations for $\widetilde{c^2}$ and $\tilde{c}^2$ and then subtracting them [38]. Following this method, the transport equation for σ_c^2 in the LES framework is obtained as

$$
\underbrace{\frac{\partial \overline{\rho}\sigma_c^2}{\partial t}}_{T_1} + \underbrace{\nabla \cdot \overline{\rho}\widetilde{\mathbf{u}}\sigma_c^2}_{T_2} = \underbrace{2(\overline{\dot{\omega}c} - \overline{\dot{\omega}}\tilde{c})}_{T_{\text{chem}}} \underbrace{-2\left(\overline{\rho D \nabla c \cdot \nabla c} - \overline{\rho}\widetilde{D}\nabla\tilde{c}\cdot\nabla\tilde{c}\right)}_{T_{\text{diss}}}
$$

$$
+ \underbrace{\nabla \cdot \left(\overline{\rho D \nabla c^2} - \overline{\rho D}\nabla\tilde{c}^2\right) + 2\tilde{c}\nabla \cdot \left(\overline{\rho D \nabla\tilde{c}} - \overline{\rho D \nabla c}\right)}_{T_{\text{diff}}}
$$

$$
\underbrace{-\nabla \cdot \left(\overline{\rho\mathbf{u}c^2} - \overline{\rho}\widetilde{\mathbf{u}}\widetilde{c^2}\right) + 2\nabla \cdot \left(\overline{\rho}\widetilde{\mathbf{u}c}\tilde{c} - \overline{\rho}\widetilde{\mathbf{u}}\tilde{c}^2\right)}_{T_{\text{tran}}} \underbrace{-2\nabla\tilde{c} \cdot (\overline{\rho}\widetilde{\mathbf{u}c} - \overline{\rho}\widetilde{\mathbf{u}}\tilde{c})}_{T_{\text{prod}}}
$$

(2)

where $\mathbf{u}$ is velocity vector, $\dot{\omega}$ is the chemical source term of c and D is the diffusion coefficient of c. The two terms on the left hand side (LHS) are unsteady and advective terms, while the terms on the right hand side (RHS) represent SGS chemical processes, dissipation of σ_c^2, diffusion, and SGS transport and production of σ_c^2 through interaction of the SGS scalar flux and the gradient of $\tilde{c}$. The dissipation term will be expressed here for convenience as $T_{\text{diss}} = -2\overline{\rho}\widetilde{\varepsilon}_c$, where $\widetilde{\varepsilon}_c$ is the SGS scalar dissipation rate (SDR).

The terms on the RHS of Equation (2) need model closure in LES frameworks. The focus here is on the importance of the SDR and how this quantity balances out the chemical, production and transport terms at high Karlovitz numbers. Exact forms of all terms will be computed directly from DNS, while T_{diss}, T_{chem} and T_{prod} will also be compared with existing model closures in order to assess how these capture the related physics at different Karlovitz numbers and filter sizes.

The production term T_{prod} is often closed using a gradient hypothesis, $\overline{\rho}\widetilde{\mathbf{u}c} - \overline{\rho}\widetilde{\mathbf{u}}\tilde{c} \approx -\nu_{SGS}\nabla\tilde{c}/\text{Sc}$, where ν_{SGS} is the SGS viscosity and $\text{Sc} \approx 0.7$ is the SGS Schmidt number. The SGS viscosity is modelled using the Smagorinsky model,

$$
\nu_{SGS} = C_s^2 \Delta^2 (\overline{S}_{ij}\overline{S}_{ij})^{1/2}
$$

(3)

where $C_s = 0.17$ is a model constant [36,39]. The reaction term will be compared with that obtained using a tabulated chemistry model [25]

$$
\overline{\dot{\omega}c} - \overline{\dot{\omega}}\tilde{c} \approx \overline{\rho}\int_0^1 \frac{\dot{\omega}_L\zeta}{\rho}\widetilde{P}(\zeta;\tilde{c},\sigma_c^2)\,\mathrm{d}\zeta - \overline{\rho}\tilde{c}\int_0^1 \frac{\dot{\omega}_L}{\rho}\widetilde{P}(\zeta;\tilde{c},\sigma_c^2)\,\mathrm{d}\zeta
$$

(4)

Here, $\dot{\omega}_L$ is the reaction rate of c in a one-dimensional unstrained laminar flame, ζ is the sample space variable for c and the PDF $\widetilde{P}$ is presumed using a β-distribution as in [25].

The modelling of the SGS scalar dissipation rate, $\widetilde{\varepsilon}_c$, is particularly challenging as the dissipation rate is related to reaction and is influenced by turbulence in premixed combustion. A first straightforward approach to close this term is to use a linear relaxation

model:

$$\widetilde{\epsilon}_c = \frac{\nu_{SGS}}{\text{Sc}A\Delta^2}\sigma_c^2 \tag{5}$$

where $A = 0.5$ is a model constant [40] and Δ is the LES filter width. This model is derived by assuming local equilibrium corresponding to a balance between dissipation and turbulent production of the SGS variance and thus it does not account for the effect of chemical reaction. This may result in an underestimation of $\widetilde{\varepsilon}_c$ as was observed in [25]. However, at large Karlovitz numbers T_{prod} becomes large and thus a linear relaxation model may be justified. This is investigated using an order of magnitude analysis (OMA) discussed in the next section. An alternative model for $\widetilde{\varepsilon}_c$ which takes into account both turbulent production and chemical reaction in the balance was proposed in [41] and successfully used in the past LES works (see for example [42–44]). This model is written as

$$\widetilde{\varepsilon}_c = \left[1 - \exp\left(-0.75\frac{\Delta}{\delta_{th}}\right)\right]\left[(2K_c - \tau C_4)\frac{S_L}{\delta_{th}} + C_3'\frac{\epsilon_k}{k}\right]\frac{\sigma_c^2}{\beta_c} \tag{6}$$

where k is the SGS turbulent kinetic energy with a dissipation rate ϵ_k, and it is computed directly from DNS in this work, and $K_c = 0.79\tau$, where $\tau = (T_b - T_u)/T_u$ is the heat release parameter. Laminar flame speed, S_L, thermal thickness, δ_{th}, and the heat release parameter, τ, are obtained from unstretched laminar flame calculations. The model constants in Equation (6) are derived from DNS studies [41] and are non-tuneable, with the possible exception of β_c. The sub-grid SDR must also be proportional to a sub-grid flow dissipation time scale and this is given by the term involving $C_3' \approx 1.2\sqrt{K_\Delta}/(1 + \sqrt{K_\Delta})$ in Equation (6), where the parameter $K_\Delta = \sqrt{\epsilon_k \delta_{th}}/S_L^{3/2}$. The factor C_4 also depends on K_Δ as $C_4 = 1.1/(1 + K_\Delta)^{0.4}$ and β_c is a model parameter with the value 2.4. The term in the first bracket of Equation (6) ensures that $\widetilde{\varepsilon}_c$ disappears in the limit of small filters while the first and second term in the second bracket represent chemical and turbulent processes, respectively. The presented models for the reaction and SDR terms are evaluated in Section 4.

3.1. *Order-of-magnitude analysis*

Order-of-magnitude analysis of the variance equation was performed in the RANS context in [45,46], and in the LES context in [25]. These analyses found that, at large Da, the reaction and dissipation terms are the leading terms, while in the low Da limit turbulence production and dissipation are leading. The analysis in [45,46] was performed using flame scales and turbulence integral scales. However, in the LES context, gradients of filtered quantities should be considered to scale with the filter size Δ, as was done in [25], and the relative magnitude of several of the terms are found to depend on Δ.

In the OMA presented in [25], the various terms in Equation (2) were scaled by $\rho_u S_L/\delta_{th}$ to enlighten the dependence on Da_Δ, the Damköhler number at the filter scale. For the scope of this work, the OMA is re-written in terms of the Karlovitz number in order to highlight the dependence on this parameter. Following the arguments in [25], the terms in Equation (2) are scaled as follows: The density, spatial derivatives of filtered quantities, the time derivative and the molecular diffusivity are scaled by ρ_u, Δ, Δ/U_{ref} and $S_L\delta_{th}$, respectively, where U_{ref} is a reference velocity associated to the large scales. The chemical reaction rate is scaled with $\rho_u S_L/\delta_{th}$ and the velocity in the turbulent transport and production terms is scaled with u'_Δ. Here $u'_\Delta = \sqrt{2k_\Delta/3}$ is a velocity associated to the filter scale and k_Δ is the sub-grid turbulent kinetic energy.

To bring Ka into the analysis, Ka has to be expressed in terms of the quantities used for the scaling. To derive a suitable expression, it is assumed that the Reynolds number is sufficiently large for the inertial range to exist, and that the filter width Δ is within this range. In this case, the Kolmogorov time scale scales as $\tau_k \sim \tau_0 \mathrm{Re}^{-1/2}$ and the chemical time scale scales as $\tau_c \sim \delta_{th}/S_L$. The time scale associated to the filter scale, $\tau_\Delta = \Delta/u'_\Delta$, can be related to the integral scales by $\tau_\Delta \sim \tau_0 (\Delta/\ell_0)^{2/3}$ [36] where τ_0 and ℓ_0 are the time and length scales associated to the integral scale. The integral time scale can then be related to the filter scales by $\tau_0 \sim (\Delta/u'_\Delta)(\ell_0/\Delta)^{2/3}$. Now the Karlovitz number can be expressed as

$$\mathrm{Ka} = \frac{\tau_c}{\tau_k} \sim \frac{\delta_{th}\mathrm{Re}^{1/2}}{S_L \tau_0} \sim \frac{\delta_{th}}{S_L}\mathrm{Re}^{1/2}\frac{u'_\Delta}{\Delta}\left(\frac{\Delta}{\ell_0}\right)^{2/3} \tag{7}$$

By using $\eta \sim \mathrm{Re}^{-3/4}\ell_0$ where η is the Kolmogorv length scale [36], one finally obtains

$$\mathrm{Ka} \sim \frac{\delta_{th}u'_\Delta}{S_L\Delta}\left(\frac{\Delta}{\eta}\right)^{2/3} = \frac{\delta_{th}u'_\Delta}{S_L\Delta}\Delta_k^{2/3} \tag{8}$$

where a normalised filter size has been defined as $\Delta_k = \Delta/\eta$. In order to expose the dependence on Ka in Equation (2), it is convenient to bring out the factor $\rho_u S_L/(\delta_{th}\Delta_k^{2/3})$ from all the terms, rather than $\rho_u S_L/\delta_{th}$ as was done in [25]. Using the previously described scalings and Equation (8) one obtains the following order of magnitudes (after dropping the leading factor $\rho_u S_L/(\delta_{th}\Delta_k^{2/3})$):

$$T_1 \sim T_2 \sim \mathcal{O}\left(\frac{U_{\mathrm{ref}}}{u'_\Delta}\mathrm{Ka}\right) \quad T_{\mathrm{diff}} \sim \mathcal{O}\left(\frac{\mathrm{Ka}}{\mathrm{Re}_\Delta}\right)$$

$$T_{\mathrm{diss}} \sim \mathcal{O}\left(\Delta_k^{2/3}\right) \quad T_{\mathrm{chem}} \sim \mathcal{O}\left(\Delta_k^{2/3}\right)$$

$$T_{\mathrm{tran}} \sim \mathcal{O}(\mathrm{Ka}) \quad T_{\mathrm{prod}} \sim \mathcal{O}(\mathrm{Ka}) \tag{9}$$

where $\mathrm{Re}_\Delta = u'_\Delta\Delta/(\delta_{th}S_L)$ is the Reynolds number at the filter scale. In Equation (9), the sub-grid scalar dissipation rate in T_{diss} is scaled using the chemical time scale, $1/\tilde{\varepsilon}_c \sim \delta_{th}/S_L$. In case the turbulent time scale τ_Δ is used instead, which may be appropriate at very high Ka, T_{diss} would instead scale as

$$T_{\mathrm{diss}} \sim \mathcal{O}\left(\frac{\rho_u S_L}{\delta_{th}\Delta_k^{2/3}} \cdot \mathrm{Ka}\right) \tag{10}$$

Due to the use of the filter size Δ_k in the scaling the terms in the above OMA should only be evaluated in relation to one another. For example, if Δ_k is increased and everything else is fixed, Equation (9) predicts that the relative importance of T_{diss} and T_{chem} compared with the other terms increases, while the absolute magnitude of T_{diss} and T_{chem} is unaffected. The following comments are made with this in mind.

The appearance of Re_Δ in the scaling for T_{diff} implies that, for a fixed Ka, this term is negligible with respect to the turbulent transport term T_{tran} as one would expect. Unsteady and advective terms are instead never negligible even at small Ka unless the characteristic velocity of the flow is very small. Furthermore, the following points can be made using Equation (9): (i) the reaction term, T_{chem}, does not increase with Ka like many other terms do, and it becomes negligible only when Ka is large and Δ_k is small. This means that, for

a fixed Ka, T_{chem} can be neglected only if the LES resolution is high enough. As will be seen in the next section, at Ka = 800, a filter size much smaller than the flame thickness is required for this to happen. (ii) The turbulent production and transport terms become large at high Ka as one would expect. This implies that the dissipation term mainly balances the reaction term at low Ka, while at intermediate and high Ka regimes the dissipation must balance the production, transport and chemical reaction terms, whose relative importance depends on Δ_k and Ka.

It is worth to note that all of the terms in Equation (2) must necessarily disappear as $\Delta \to 0$, indicating that the scaling above may only be valid at sufficiently large Δ_k where the filter operation has a significant effect.

After predicting the behaviour of the various terms by means of the above order of magnitude analysis, it would be interesting to observe the behaviour of the various terms in Equation (2) while varying Ka and Δ when the length scale (η or ℓ_0 for example) is fixed, and in particular to observe the behaviour of term T_{diss} from DNS and how it compares to its modelling when different assumptions are made. This is the topic of the next section.

4.　Results and discussion

DNS data is used in the first half of this section to compare the behaviour and relative importance of the various terms in Equation (2) at different Karlovitz numbers and filter sizes in the light of the observations made in OMA. In the second part of this section the models described in Section 3 are evaluated.

When various quantities ψ are presented as conditional averages on $\tilde{c}$ the following definition is used:

$$\langle \psi \mid \tilde{c} = c^* \rangle = \frac{\int_{t_1}^{t_2} \iiint_V \psi(\mathbf{x}, t) \cdot I_{c,\delta} \, d\mathbf{x} \, dt}{\int_{t_1}^{t_2} \iiint_V I_{c,\delta} \, d\mathbf{x} \, dt} \tag{11}$$

In Equation (11), t_1 and t_2 are the times at which the sampling starts and ends, V is the computational domain and $I_{c,\delta} = H(\tilde{c} - c^* + \delta) - H(\tilde{c} - c^* - \delta)$ is a rectangular window function where H is the Heaviside function. The parameter δ, representing half the bin size, has a finite value of $\delta = 1/80$ resulting in a coarse-grained average.

When different filter sizes are used, the largest meaningful filter is limited by the cross-stream domain size. Since the domain size is fixed at 5.5 times δ_{th} for all simulations presented here, the largest filter corresponds to a fixed value of $\Delta^+ = \Delta/\delta_{th} \approx 5$ for all cases. However, the largest meaningful filter size in terms of Δ_k, which is normalised by the Kolmogorov scale, is case dependent and ranges from about 50 for case K4 to about 1200 for case K4100. It is sometimes convenient to use Δ^+ but the two filter sizes are simply related by $\Delta^+ = \Delta_k \cdot \eta/\delta_{th}$ (cf. Table 1 for the values of η/δ_{th}). For a fixed Ka, an increase of Δ^+ corresponds to an increase of Δ_k. An increase in Ka for a fixed Δ^+ also results in an increase of Δ_k. For example, the filter size of $\Delta^+ = 3.5$ corresponds roughly to a Δ_k of 35, 130, 300 and 700 for cases K4, K100, K800 and K4100, respectively.

Each of the simulations was performed over at least 20 integral time scales τ_0, and t_1 and t_2 were set to include only the last 10 integral time scales of each simulation to remove the initial transient stage from the statistical analysis. This was decided based on the time evolution of the terms T_{chem}, T_{prod} and T_{diss}, which is shown in Figure 4 for $\Delta^+ = 1.0$ and conditioned on $c = 0.3$ and $c = 0.7$. The integral time scale is estimated as $\tau_0 = \ell_0/u'$. As a verification of the numerical accuracy of the post-processing, all terms of Equation (2)
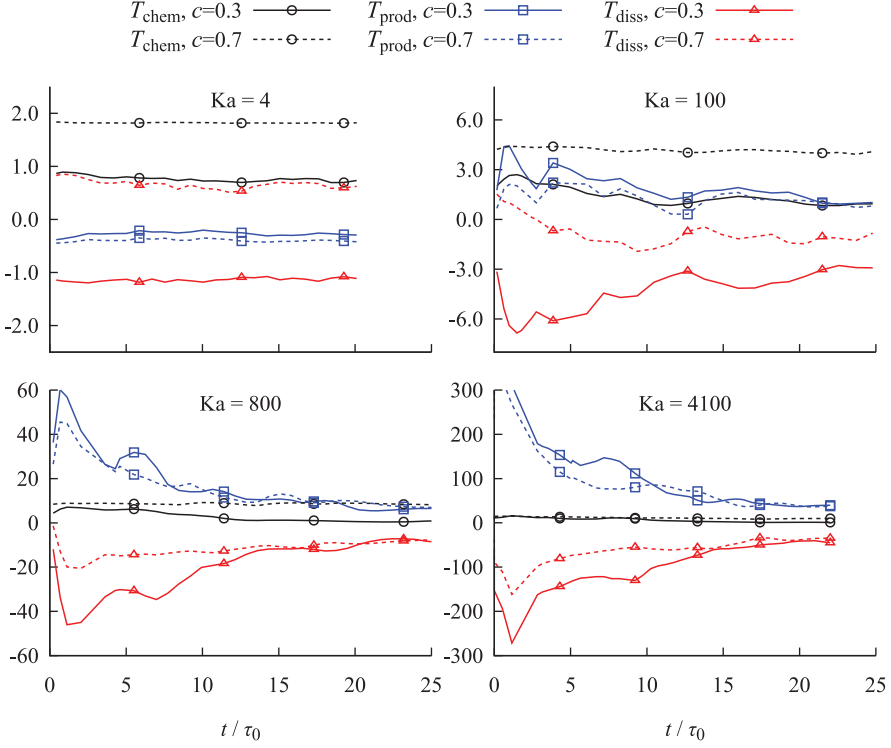
Figure 4. Time evolution of T_{chem}, T_{prod} and T_{diss} conditioned on $c=0.3$ and $c=0.7$ for $\Delta^+ = 1.0$. The terms are normalized by $\rho_u S_L/\delta_{th}/\Delta_k^{2/3}$.

were computed independently to calculate the imbalance (difference between left and right hand side of the equation). This maximum imbalance occurs for the K4100 case and is not larger than 5% of the peak value of T_{diss}.

4.1. *DNS analysis of the variance equation*

The exact form of the RHS terms of Equation (2) computed from the four DNS flames is shown in Figure 6 as conditional averages. Three filter sizes are shown for each Ka, which are $\Delta^+ = 0.35$, 1.0 and 3.5. Note that the unsteady and advective terms, T_1 and T_2, which are in closed form in Equation (2), are excluded for clarity. To provide a direct measure of the relative importance of the different terms in Equation (2), in addition to the conditional averages, Figure 5 shows the integrated magnitude of each term normalized by the total magnitude of all terms as function of filter size Δ_k. This measure will be referred to as I and for a term T_k it is defined by

$$I_k = \frac{\int_{t_1}^{t_2} \iiint_V |T_k| \, d\mathbf{x} \, dt}{\sum_i \int_{t_1}^{t_2} \iiint_V |T_i| \, d\mathbf{x} \, dt} \tag{12}$$

In Equation (12), the sum is taken over all the terms T_{diff}, T_{chem}, T_{diss}, T_{prod}, T_{tran} and T_{1+2} where $T_{1+2} = T_1 + T_2$ is the sum of the transient and advective terms. Figures 5 and 6 are complementary; Figure 5 shows which of the unclosed terms makes the largest
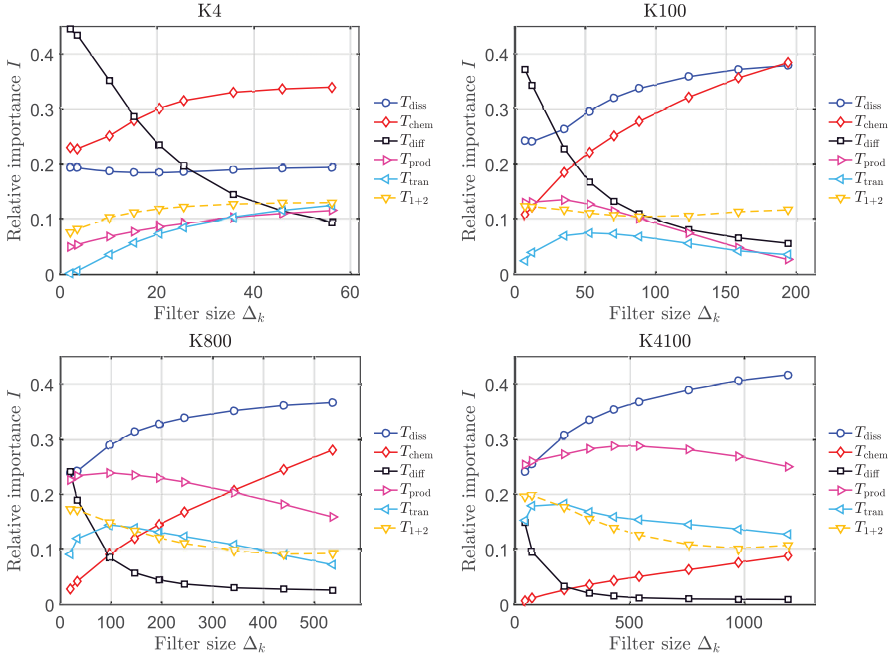
Figure 5. Relative importance of all terms in the variance equation as function of the filter size Δ_k for the four cases.

contributions to the budget, and are therefore most important to model, under different conditions while Figure 6 shows how the terms vary with c.

The molecular diffusion term, T_{diff}, is found to be important for small filter sizes but loses its importance as the filter size is increased. In the parameter range accessed by the present data, T_{diff} is one of the terms that shows the largest variations. For example, for small filters in cases K4 and K100, it is the dominating term while for large filters in cases K800 and K4100, it is the smallest term and contributes less than 5% of the budget (as measured by the relative importance I defined above). The decrease with filter size is explained by the appearance of Re_Δ in the scaling as seen in the order of magnitude analysis. In Figure 6, it is seen that the diffusion term T_{diff} acts as a source term for $\tilde{c} < 0.5$ and as a sink term for $\tilde{c} > 0.5$.

The chemical term, T_{chem}, is seen to increase in importance with increasing filter size for all cases. This is consistent with the Δ_k-scaling predicted by the OMA in Equation (9). When discerning the trend with changing Ka at a fixed filter size the comparison is limited to values of Δ_k that are available for several of the plots in Figure 5. Comparison at fixed Δ_k shows that the chemical term T_{chem} loses importance with increasing Ka but remains important up to Ka= 800 for the filter sizes investigated. This suggests that, for any given Ka, there exists a filter size above which T_{chem} will be important when modelling the sub-grid variance equation.

For the dissipation term, T_{diss}, the situation is similar to that of T_{chem}. The relative importance increases with increasing Δ_k but with the exception of case K4 in which the importance is constant. The dissipation term gains importance going from case K4 to case K100 but apart from that there is no clear trend with increasing Ka. Furthermore, it is seen in both Figures 6 and 5 that T_{diss} remains one of the most important terms at almost
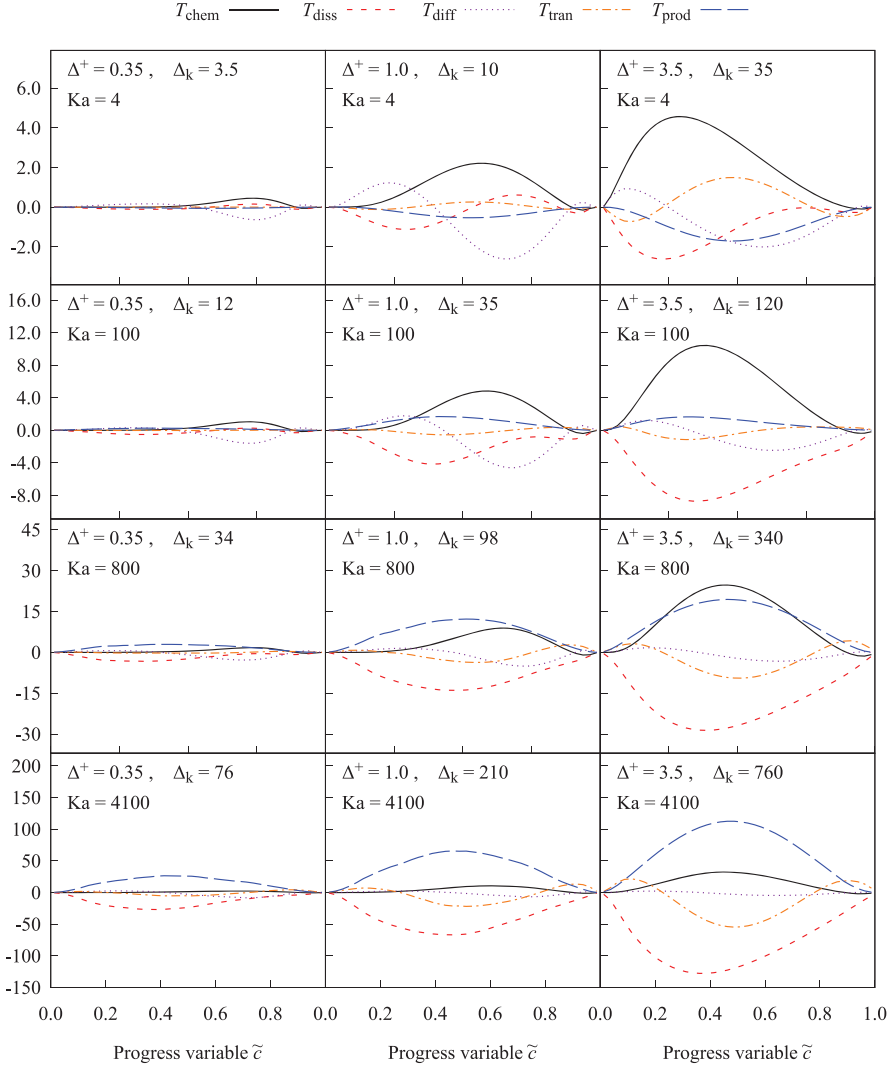
Figure 6. Conditional averages of the terms in variance equation. Four cases (top to bottom: K4, K100, K800, K4100) and three filter sizes (left to right: $\Delta^+ = 0.35$, 1.0 and 3.5) are shown. All terms are normalized by $\rho_u S_L / \delta_{th} / \Delta_k^{2/3}$.

all investigated Ka and filter sizes; it is notable that its relative importance does not drop lower than $\sim 20\%$ for any investigated combination of Ka and Δ_k while all other terms do at least at some point drop below 10%. This observation gives some support to the alternative scaling presented in Equation (10) where it was predicted that T_{diss} scales with Ka if the chemical time scale is long. If T_{diss} did not scale with Ka then it would lose importance to other terms that do have this scaling.

It may be expected that T_{diss} should be everywhere negative, as it is for constant density flow. This is not the case when density-weighted Favre filtering is used, however, and this is seen in Figure 6 for small filter sizes in mainly the K4 case where the appearance of positive values of the dissipation term is evident. This can be understood by inspecting T_{diss} which

is of the form $\widetilde{\nabla c \nabla c} - \nabla \tilde{c} \nabla \tilde{c}$. If the filter operator were to commute with the gradient in the second term in this expression, as an unweighted filter does, then the positiveness of the expression follows from Cauchy-Schwarz inequality. However, since the density-weighted filter operation, which does not commute with the gradient, is used here there is no mathematical guarantee of the positiveness of this term. Thus, positive values of T_{diss} does occur in some cases and are mainly seen in laminar or weakly turbulent flames for small filters.

The remaining terms T_{prod}, T_{tran} and T_{1+2} were all predicted to scale as Ka in the OMA with no particular dependence on Δ_k. The relative importance of these terms, however, does drop for large filter sizes due to the concurrent increase of the dissipation and reaction terms as seen in Figure 5. At low Ka (cases K4 and K100), the three terms are of comparable importance but at high Ka (K800 and K4100) the production term T_{prod} stands out as the largest and it can reach an importance I above 25% for case K4100. This shows that modelling of the production term is especially relevant at high Ka.

From Figure 6, it is also seen that the profiles of turbulent transport (T_{tran}) and turbulent production (T_{prod}) have opposite sign at small Ka compared with that at high Ka. In fact, the production term acts as a sink term at Ka = 4, although the sum of T_{prod} and T_{tran} remains positive. The changing sign of the production term does make it more challenging to model.

From the modelling perspective, it is important to know which of the unclosed terms dominates for different flames and filter sizes. Referring to the order-of-magnitude analysis (Equations. (9)–(10)) as well as Figure 5, the following can be concluded: In the limit of large Δ_k, for a fixed Ka, there will be a balance of dissipation and chemical reaction (as well as transient and advective terms T_1 and T_2). In the limit of large Ka, for a fixed Δ_k, there will be a balance of dissipation and production. It should be kept in mind, however, that the latter limit may not be practically realisable since the resolution requirement, e.g. in terms of the 80% resolved kinetic energy criterion [36], to maintain Δ_k constant with increasing Ka would imply refining the grid and thus increase the computational cost. In most practical LES, the filter size is larger than the flame thickness, $\Delta^+ > 1$, and T_{chem} will be non-negligible except in the case of both very high Ka and high resolution (small Δ_k). For most LES, the filter size also fulfils $\Delta_k \gg 1$ so that, at high Ka, all terms except molecular diffusion (T_{diff}) will have significant contributions.

Some further insight can be found for the dissipation term T_{diss} in Figure 6. This term, which is the main sink in Equation (2), must balance the contributions coming from turbulent production and chemical reaction, which are the main source terms. According to the observed relative magnitude between T_{chem} and T_{prod}, the dissipation term increases in magnitude with the filter size and becomes rather independent of Ka for low and intermediate values of Ka. This is because at these Ka the SGS scalar dissipation rate $\widetilde{\varepsilon}_c$, appearing in T_{diss}, is more likely to scale with the inverse of a chemical time scale, as discussed in Section 3.1. At very high Ka, in combination with small Δ^+, the turbulent time scale τ_Δ becomes a more relevant scale for $\widetilde{\varepsilon}_c$ and eventually T_{diss} is balanced entirely by the production term T_{prod}. This suggests that a linear relaxation model for T_{diss} would be appropriate in the limit of very high Ka.

4.2. *Modelling of the variance equation*

As discussed in the previous subsection, the relative magnitudes of the production, dissipation and chemical reaction terms (T_{prod}, T_{diss} and T_{chem}) in the SGS variance equation,

Equation (2), depend on Ka and at high Ka they can all be significant. This has to be captured in LES modelling and it is thus of interest to explore how common LES closures for these three terms perform at different Ka and filter sizes.

4.2.1. *Modelling of the dissipation term*

The dissipation term, T_{diss}, is seen to always be of significant magnitude. A comparison of two common LES closures, defined in Equations (5) and (6), for T_{diss} in the context of $\tilde{c}$-modelling is presented next. In Figure 7, the dissipation term T_{diss} (square symbols)
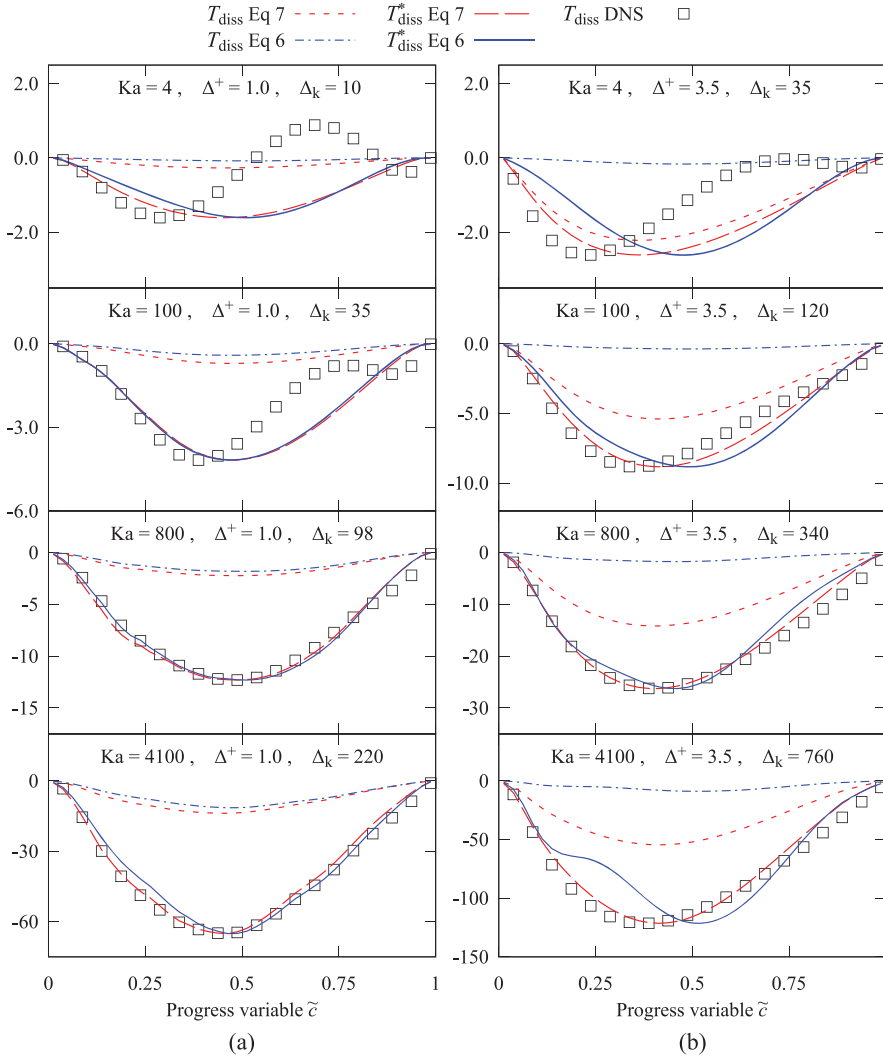

Figure 7. Conditional variations of T_{diss} (squares) compared with the models of Equation (5) and (6) (dashed lines). The solid lines show scaled versions of the models, normalised to match the DNS peak value. The filter size is (a)$\Delta^+ = 1.0$ and (b) $\Delta^+ = 3.5$. Corresponding values of Δ_k are given in the figure. The terms are normalized by $\rho_u S_L / \delta_{th} / \Delta_k^{2/3}$.

obtained from DNS is compared with those computed using the linear relaxation model, Equation (5) (dash-dotted lines), and that proposed by Dunstan et al. [41], Equation (6) (short-dashed lines). The terms are shown as conditional averages for the four different cases and two filter sizes, $\Delta^+ = 1.0$ and 3.5. In the figure, the filter size is also given in terms of Δ_k based on η in the upstream turbulence in the unburned mixture for each case. First, one can notice that the dissipation term is severely under-predicted by the linear relaxation model for all Karlovitz numbers and both filter sizes; this may be explained by the fact that this model was not intended for reactive scalars and an adjustment of the model constant A can therefore be motivated. Comparison of the short-dashed lines and squares in Figure 7 indicates that the model given by Equation (6) does capture the right order of magnitude for the larger filter size, although under-prediction occurs for small filters and to some extent also for larger Ka. This shows that scaling of the model constants, β_c and A, is relevant for practical LES. The models depend on Δ and Ka and they have to be chosen carefully in an LES. Their value can be found using, when possible, a dynamic approach as was done for β_c in [25], or choosing the constant from a DNS database. How to optimally scale these constants is not the focus here and will be the topic of a future study.

The ability of the dissipation term closures to reproduce the right profile in the $\tilde{c}$-coordinate is instead explored next. In order to compare the shape of the profiles, the modelled dissipation terms are scaled to match the peak magnitude of T_{diss} from the DNS. The scaled terms are denoted T_{diss}^* and are shown as solid and long-dashed lines in Figure 7. From the plots, it is seen that both models predict the shape well, except at the combination of low Ka and small filter where both models fail and the combination of large filter and very high Ka where Equation (5) tends to predicts a peak position shifted towards higher $\tilde{c}$. Overall the functional form of Equation (5) seems to be more prone to error and predictions from the scaled Equation (6) remain more accurate as this model accounts for chemical processes.

For the scaled plots of Equation (6) in Figure 7, it can be inferred that the model constant, β_c, depends on Δ^+ and Ka. Figure 8 shows how the model constants β_c and A vary with Ka, Δ^+ and Δ_k. It is seen that β_c increases with increasing Δ^+ and Δ_k; this trend is true for the full range of Δ^+ and Ka accessible by the current data. Also, for filter sizes $\Delta^+ > 1$, the value of β_c decreases with increasing Ka. This trend of β_c is consistent with the physical definition of this parameter. Indeed, β_c can be defined as [2,47]:

$$\beta_c \frac{\bar{\rho}\tilde{\epsilon}_c^2}{\sigma_c^2} = -\underbrace{2\mathcal{D}(\nabla c \cdot \nabla \dot{\omega}_c)}_{T_4} + \underbrace{2\rho\mathcal{D}^2(\nabla\nabla c : \nabla\nabla c)}_{D_2} \tag{13}$$

Thus, β_c is strongly influenced by the curvature of the flame (through D_2) and ∇c and $\nabla\dot{\omega}_c$. As Ka increases, the curvature of the flame increases due to the intense turbulence which leads to an increase in D_2, while the flame thickness induces a decrease in T_4 (as ∇_c and $\nabla\dot{\omega}_c$ decreases). This then leads to a decrease in β_c. The corresponding trends for the parameter A in Equation (5) are not as regular, in particular the K4 case shows a deviating behaviour, but it can be seen that A does decrease with Δ^+ and Δ_k for Ka ≥ 100. As a function of Ka, A is decreasing for large filters and remains constant or slowly increasing for small filters. For the most part, A shows an opposite trend to β_c variations.

4.2.2. *Modelling of the chemical reaction term*

For practical values of Δ^+, the magnitude of the dissipation term, T_{diss}, is strongly influenced by the reaction term at low Ka and by a combination of reaction and turbulent
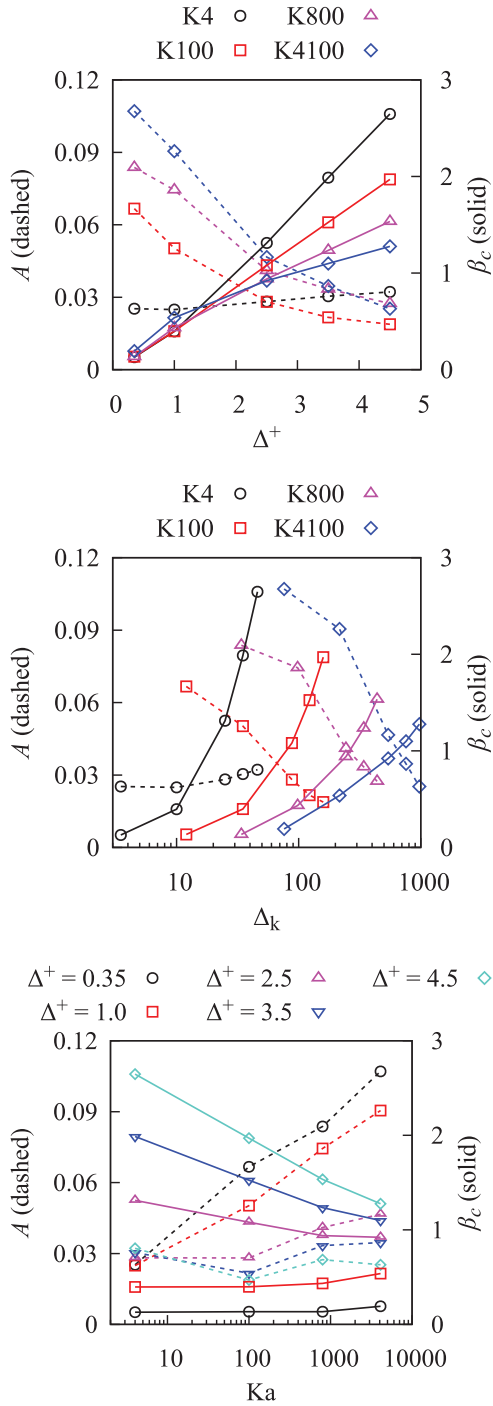
Figure 8. Values of the model constants β_c (solid lines) and A (dashed lines) after scaling to match the peak value to the DNS result. The figure shows the dependence of these model constants on Δ^+, Δ_k and Ka.
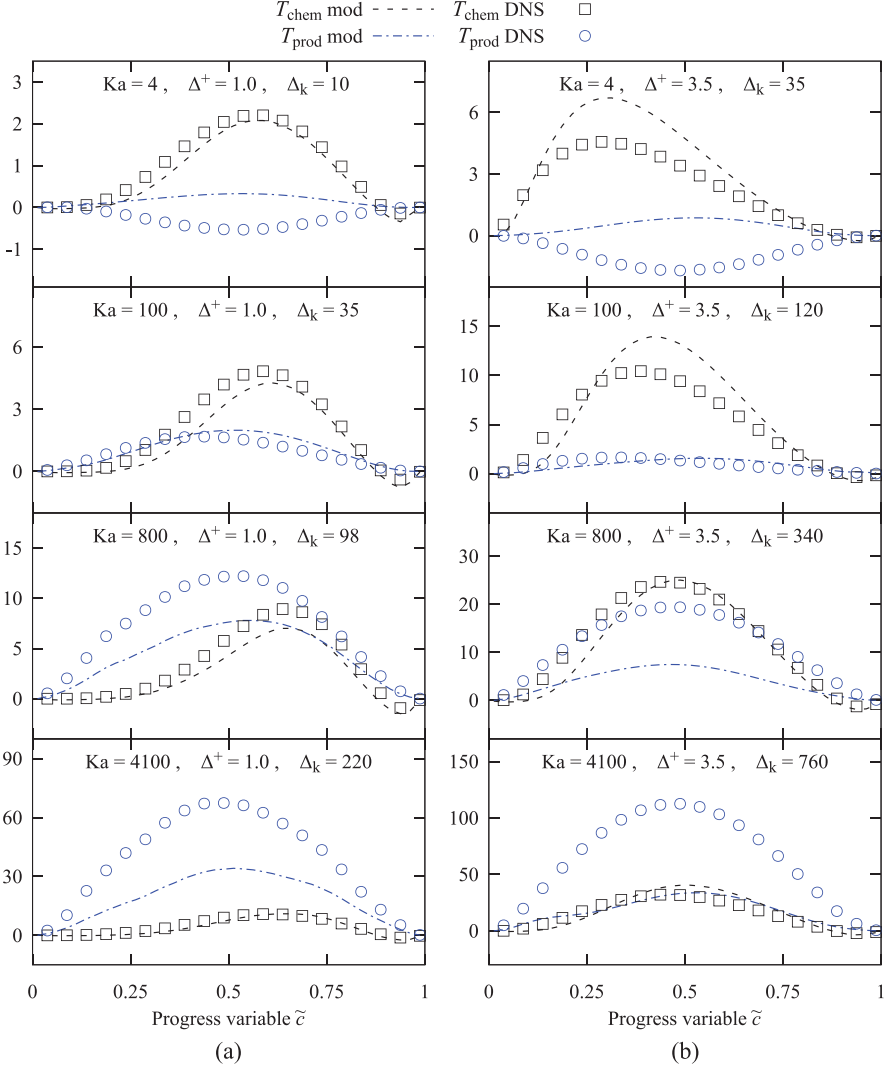
Figure 9.   Conditional variations of T_{chem} (squares) and T_{prod} (circles) compared with corresponding models (dashed lines). The filter size is (a) $\Delta^+ = 1.0$ and (b) $\Delta^+ = 3.5$. Corresponding values of Δ_k are given in the figure. The terms are normalized by $\rho_u S_L/\delta_{th}/\Delta_k^{2/3}$.

production at higher Ka as discussed in Section 4.1. Modelling the dissipation term accurately is not sufficient if the reaction term is not modelled with similar accuracy, as the balance between dissipation, turbulent production and chemical reaction would be affected by an incorrect estimation of T_{chem}. In Figure 9, a comparison between the reaction term T_{chem} from DNS (squares) and that obtained using the tabulation approach of Equation (4) (dashed line) is shown. This closure seems to predict the term T_{chem} well at high Ka but a discrepancy can be observed for Ka 4 and 100 for the larger filter size. The maximum error is observed to be about 25% near the peak at Ka = 4 and 100 for $\Delta^+ = 3.5$. Past studies [48,49] showed that higher errors due to the beta-PDF can be expected for low

Ka. However, the error is again lower for larger Ka (800 and 4100), suggesting that this evaluation is not straightforward. Additional studies will be needed to shed light on this non-trivial behaviour.

4.2.3. *Modelling of the turbulent production term*

Finally, the modelling of the turbulent production term T_{prod} is assessed using a gradient hypothesis. In Figure 9 conditional averages are shown for T_{prod} obtained from DNS (circles) as well as the gradient hypothesis model (dot-dashed lines). In case K4, this hypothesis does not work and the model ends up predicting the wrong sign due to negative correlation. In case K100, the model seems to work well. For even higher Ka considerable under-prediction is observed.

However, at the higher Ka, 800 and 4100, the model prediction does improve when the filter size is decreased and the best match is observed for the combination $\Delta^+ \leq 1$ and Ka$\geq$ 100. While it is not certain why the prediction is poor with a large filter size, some reasons that may play a role include: over-estimation of the turbulent Schmidt number that leads to too small production, and the use of filter sizes comparable to the integral scale. It is possible that dynamic approaches for ν_{SGS} and Sc may improve the prediction of T_{prod}, a topic that deserves further study.

5. Conclusions

Direct numerical simulations of premixed methane-air flames for low and high Ka have been performed to investigate the behaviour of different terms in the transport equation for progress variable SGS variance in different combustion regimes. This equation is of particular relevance for progress variable-based models in LES frameworks. The relative scaling of these terms was also analysed by an order-of-magnitude analysis. Moreover, the accuracy of two common LES closures of the scalar dissipation term as well as closures for the chemical reaction and turbulent production terms were assessed at both low and high Ka for different normalised filter sizes Δ_k. The main results are summarised in the following.

- The relative importance of the chemical term decreases with Ka and increases with Δ_k. Both the DNS data and the order-of-magnitude analysis supports this result. The importance of the chemical term must be considered in relation with LES resolution and under a combination of both high Ka and large Δ_k this term can be important. It is observed that, at a Ka of 800, the chemical term is one of the largest terms for filter sizes of the order of the laminar flame thickness or larger. At Ka as high as 4100, the chemical term is still seen to gain significance with Δ for all filter sizes accessible with the current data. It is implied that the chemical term is non-negligible for most practical combinations of Ka and Δ. It was also seen that a simple tabulation approach can model the chemical term well at all investigated filter sizes and Karlovitz numbers.
- Molecular diffusion in the variance equation is an important term only for small filters and low Ka. The term was observed to contribute as much as 40% of the budget in a case with small filter and low Ka, while it made a negligible contribution in a case with large filter and high Ka.
- The turbulent transport and production terms gains higher relative importance when Ka increases. This conclusion is supported by the DNS data and the OMA. It was also

found, however, that the production term changes sign and becomes a sink term at small Ka. Modelling of the production term by a gradient transport approximation with the sub-grid viscosity estimated by a constant coefficient Smagorinsky model was found to be insufficient in most cases. Further studies, including dynamic modelling approaches, will be needed for this term.

- The dissipation term is the main sink term in the variance equation, except in some cases with small filters where molecular diffusion can also be an important sink. Since the dissipation term on average has to balance the sources due to turbulent production and chemical reaction, the dissipation term ends up being always one of the leading terms. At high Ka, when the Kolmogorov time scale is short compared with the chemical time scale, the relative importance of the dissipation term also changes from a scaling with filter size at low Ka to a scaling with Ka at high Ka. The modelling of the dissipation term is therefore crucial and needs to account for both turbulent and chemical processes. Two different closures were compared for the dissipation term, including the model proposed in [41] which is developed for reactive scalars, and a linear relaxation model which is commonly used for passive scalars. It was found that, while both models require their constants to be selected with care, the linear relaxation model is less likely to predict the right functional form of the conditionally averaged dissipation term. The adjusted model constant in the model from [41] also appears to follow a more consistent trend with Ka and Δ compared with the model constant of the linear relaxation model.

To conclusively confirm the trends observed in this paper, and in particular the behaviour of models, further work is needed including studies of a wider range filter sizes Δ^+, length scales ℓ_0 and flame parameters S_L, δ_{th} and τ. Dynamic approaches exist for the model constants β_c and C_s which may improve the prediction of the dissipation and production terms and reduce the need for calibration, and future work should also consider such approaches.

Disclosure statement

No potential conflict of interest was reported by the authors.

ORCID

Thommie Nilsson http://orcid.org/0000-0001-9573-0433
Nguyen Anh Khoa Doan http://orcid.org/0000-0002-9890-3173

References

[1] D. Dunn-Rankin and P. Therkelsen, *Lean Combustion: Technology and Control*, Academic Press, Boston, 2016.

[2] N. Swaminathan and K.N.C. Bray, *Turbulent Premixed Flames*, Cambridge University Press, Cambridge, 2011.

[3] T. Lieuwen, V. McDonell, E. Petersen, and D. Santavicca, *Fuel Flexibility Influences on Premixed Combustor Blowout, Flashback, Autoignition, and Stability*, J. Eng. Gas Turbines Power 130 (2008), pp. 011506.

[4] R.W. Bilger, *Future progress in turbulent combustion research*, Prog. Energy Combust. Sci. 26 (2000), pp. 367–380.

[5] B. Zhou, C. Brackmann, Q. Li, Z. Wang, P. Petersson, Z. Li, M. Aldén, and X.S. Bai, *Distributed reactions in highly turbulent premixed methane/air flames. Part I. Flame structure characterization*, Combust. Flame 162 (2015), pp. 2937–2953.

[6] M.J. Dunn, A.R. Masri, and R.W. Bilger, *A new piloted premixed jet burner to study strong finite-rate chemistry effects*, Combust. Flame 151 (2007), pp. 46–60.

[7] B. Savard, B. Bobbitt, and G. Blanquart, *Structure of a high Karlovitz n-C7H16 premixed turbulent flame*, Proc. Combust. Inst. 35 (2015), pp. 1377–1384.

[8] S. Lapointe and G. Blanquart, *Fuel and chemistry effects in high Karlovitz premixed turbulent flames*, Combust. Flame 167 (2016), pp. 294–307.

[9] A.J. Aspden, J.B. Bell, and S.E. Woosley, *Distributed flames in type Ia supernovae*, Astrophys. J. 710 (2010), pp. 1654–1663.

[10] H. Carlsson, R. Yu, and X.S. Bai, *Direct numerical simulation of lean premixed CH4/air and H2/air flames at high Karlovitz numbers*, Int. J. Hydrog. Energy 39 (2014), pp. 20216–20232.

[11] A.J. Aspden, *A numerical study of diffusive effects in turbulent lean premixed hydrogen flames*, Proc. Combust. Inst. 36 (2017), pp. 1997–2004.

[12] W.L. Roberts, J.F. Driscoll, M.C. Drake, and L.P. Goss, *Images of the quenching of a flame by a vortex—to quantify regimes of turbulent combustion*, Combust. Flame. 94 (1993), pp. 58–69.

[13] M.J. Dunn, A.R. Masri, R.W. Bilger, R.S. Barlow, and G.H. Wang, *The compositional structure of highly turbulent piloted premixed flames issuing into a hot coflow*, Proc. Combust. Inst. 32 (2009), pp. 1779–1786.

[14] A.Y. Poludnenko and E.S. Oran, *The interaction of high-speed turbulence with flames: Global properties and internal flame structure*, Combust. Flame 162 (2015), pp. 995–1011.

[15] S. Srinivasan and S. Menon, *Linear eddy mixing model studies of high Karlovitz number turbulent premixed flames*, Flow, Turbul. Combust. 93 (2014), pp. 189–219.

[16] S. Lapointe, B. Savard, and G. Blanquart, *Differential diffusion effects, distributed burning, and local extinctions in high Karlovitz premixed flames*, Combust. Flame 162 (2015), pp. 3341–3355.

[17] R. Sankaran, E.R. Hawkes, C.S. Yoo, and J.H. Chen, *Response of flame thickness and propagation speed under intense turbulence in spatially developing lean premixed methane-air jet*, Combust. Flame162 (2015), pp. 3294–3306.

[18] H. Wang, E.R. Hawkes, J.H. Chen, B. Zhou, Z. Li, and M. Aldén, *Direct numerical simulations of a high Karlovitz number laboratory premixed jet flame an analysis of flame stretch and flame thickening*, J. Fluid Mech. 815 (2017), pp. 511–536.

[19] S. Chaudhuri, H. Kolla, H.L. Dave, E.R. Hawkes, J.H. Chen, and C.K. Law, *Flame thickness and conditional scalar dissipation rate in a premixed temporal turbulent reacting jet*, Combust. Flame 184 (2017), pp. 273–285.

[20] A.J. Aspden, M.S. Day, and J.B. Bell, *Turbulence-chemistry interaction in lean premixed hydrogen combustion*, Proc. Combust. Inst. 35 (2015), pp. 1321–1329.

[21] O. Colin, F. Ducros, D. Veynante, and T. Poinsot, *A thickened flame model for large eddy simulations of turbulent premixed combustion*, Phys. Fluids 12 (2000), pp. 1843–1863.

[22] C.D. Pierce and P. Moin, *Progress-variable approach for large-eddy simulation of non-premixed turbulent combustion*, J. Fluid Mech. 504 (2004), pp. 73–97.

[23] G. Wang, M. Boileau, D. Veynante, and K. Truffin, *Large eddy simulation of a growing turbulent premixed flame kernel using a dynamic flame surface density model*, Combust. Flame 159 (2012), pp. 2742–2754.

[24] V. Moureau, B. Fiorina, and H. Pitsch, *A level set formulation for premixed combustion LES considering the turbulent flame structure*, Combust. Flame 156 (2009), pp. 801–812.

[25] I. Langella and N. Swaminathan, *Unstrained and strained flamelets for LES of premixed combustion*, Combust. Theory Model. 20 (2016), pp. 410–440.

[26] S. Lapointe and G. Blanquart, *A priori filtered chemical source term modeling for LES of high Karlovitz number premixed flames*, Combust. Flame 176 (2017), pp. 500–510.

[27] T. Nilsson, H. Carlsson, R. Yu, and X.S. Bai, *Structures of turbulent flames in the high Karlovitz number regime – DNS analysis*, Fuel 216 (2018), pp. 627–638.

[28] J. Jeong and F. Hussain, *On the identification of a vortex*, J. Fluid Mech. 285 (1995), pp. 69–94.

[29] R. Yu and N. Lipatnikov, *DNS study of dependence of bulk consumption velocity in a constant-density reacting flow on turbulence and mixture characteristics*, Phys. Fluids 29 (2017), pp. 065116.

[30] S. Ghosal, T.S. Lund, P. Moin, and K. Akselvoll, *A dynamic localization model for large-eddy simulation of turbulent flows*, J. Fluid Mech. 286 (1995), pp. 229–255.

[31] R. Yu, J. Yu, and X.S. Bai, *An improved high-order scheme for DNS of low mach number turbulent reacting flows based on stiff chemistry solver*, J. Comp. Phys. 231 (2012), pp. 5504–5521.

[32] G. Strang, *On the construction and comparison of difference schemes*, SIAM J. Numer. Anal. 5 (1968), pp. 506–517.

[33] P.N. Brown, G.D. Bryne, and A.C. Hindmarsch, *VODE, a variable-coefficient ode solver*, SIAM J. Sci. Stat. Comp. 10 (1989), pp. 1038–1051.

[34] R. Yu and X.S. Bai, *A semi-implicit scheme for large eddy simulation of piston engine flow and combustion*, Int. J. Numer. Methods Fluids 71 (2013), pp. 13–40.

[35] M. Smooke and V. Giovangigli, *Reduced Kinetic Mechanisms and Asymptotic Approximation for Methane-air Flames*, Springer-Verlag, Berlin, 1991.

[36] S.B. Pope, *Turbulent Flows*, Cambridge University Press, Cambridge, 2000.

[37] N. Peters, *The turbulent burning velocity for large-scale and small scale turbulence*, J. Fluid Mech. 384 (1999), pp. 107–132.

[38] C. Jimenez, F. Ducros, B. Cuenot, and B. Bedat, *Subgrid scale variance and its dissipation of a scalar field in large eddy simulations*, Phys. Fluids 13 (2001), pp. 1748–1754.

[39] D.K. Lilly, *The representation of small-scale turbulence in numerical experiments*, Proc. IBM Scientific Computing Symp. on Environmental Sciences, 1967, pp. 195–210.

[40] H. Pitsch, *Large-eddy simulation of turbulent combustion*, Annu. Rev. Fluid Mech. 38 (2006), pp. 453–482.

[41] T.D. Dunstan, Y. Minamoto, N. Chakraborty, and N. Swaminathan, *Scalar dissipation rate modelling for large eddy simulation of turbulent premixed flames*, Proc. Combust. Inst. 34 (2013), pp. 1193–1201.

[42] I. Langella, N. Swaminathan, and R.W. Pitz, *Application of unstrained flamelet SGS closure for multi-regime premixed combustion*, Combust. Flame 173 (2016), pp. 161–178.

[43] I. Langella, N. Swaminathan, Y. Gao, and N. Chakraborty, *Assessment of dynamic closure for premixed combustion large eddy simulation*, Combust. Theory Model. 19 (2015), pp. 628–656.

[44] Z. Chen, S. Ruan, and N. Swaminathan, *Large Eddy Simulation of flame edge evolution in a spark-ignited methane air jet*, Proc. Combust. Inst. 36 (2017), pp. 1645–1652.

[45] O.R. Darbyshire, N. Swaminathan, and S. Hochgreb, *The Effects of Small-Scale Mixing Models on the Prediction of Turbulent Premixed and Stratified Combustion*, Combust. Sci. Technol. 182 (2010), pp. 1141–1170.

[46] A.J. Aspden, M.S. Day, and J.B. Bell, *Turbulence flame interactions in lean premixed hydrogen: transition to the distributed burning regime*, J. Fluid Mech. 680 (2011), pp. 287–320.

[47] G. Ghiasi, N.A.K. Doan, N. Swaminathan, B. Yenerdag, Y. Minamoto, and M. Tanahashi, *Assessment of sgs closure for isochoric combustion of hydrogen-air mixture*, Int. J. Hydrogen Energy 43 (2018), pp. 8105–8115.

[48] B. Fiorina, R. Vicquelin, P. Auzillon, N. Darabiha, O. Gicquel, and D. Veynante, *A filtered tabulated chemistry model for les of premixed combustion*, Combust. Flame 157 (2010), pp. 465–475.

[49] I. Langella, N. Swaminathan, F.A. Williams, and J. Furukawa, *Large-Eddy Simulation of Premixed Combustion in the Corrugated-Flamelet Regime*, Combust. Sci. Technol. 188 (2016), pp. 1565–1591.